WATER RESOURCES RESEARCH, VOL. 49, 3897–3911, doi:10.1002/wrcr.20289, 2013

Transport of *E. coli* in aquifer sediments of Bangladesh: Implications for widespread microbial contamination of groundwater

John Feighery,[1] Brian J. Mailloux,[2] A. S. Ferguson,[3] Kazi Matin Ahmed,[4] Alexander van Geen,[5] and Patricia J. Culligan[3]

Received 11 February 2012; revised 7 March 2013; accepted 25 April 2013; published 3 July 2013.

[1] Fecal bacteria are frequently found at much greater distances than would be predicted by laboratory studies, indicating that improved models that incorporate more complexity might be needed to explain the widespread contamination of many shallow aquifers. In this study, laboratory measurements of breakthrough and retained bacteria in columns of intact and repacked sediment cores from Bangladesh were fit using a two-population model with separate reversible and irreversible attachment sites that also incorporated bacterial decay rates. Separate microcosms indicated an average first-order decay rate of 0.03 $\log_{10}$/day for both free bacteria in the liquid phase and bacteria attached to the solid phase. Although two thirds of the column results could be well fit with a dual-deposition site, single-population model, fitting of one third of the results required a two-population model with a high irreversible attachment rate (between 5 and 60 h^{-1}) for one population of bacteria and a much lower rate (from 5 h^{-1} to essentially zero) for the second. Inferred attachment rates for the reversible sites varied inversely with grain size (varying from 1 to 20 h^{-1} for grain sizes between 0.1 and 0.3 mm) while reversible detachment rates were found to be nearly constant (approximately 0.5 h^{-1}). Field simulations based on the fitted two-population model parameters predict only a twofold reduction in fecal source concentration over a distance of 10 m, determined primarily by the decay rate of the bacteria. The existence of a secondary population of bacteria with a low attachment rate might help explain the observed widespread contamination of tubewell water with *E. coli* at the field site where the cores were collected as well as other similar sites.

Citation: Feighery, J., B. J. Mailloux, A. S. Ferguson, K. M. Ahmed, A. van Geen, and P. J. Culligan (2013), Transport of *E. coli* in aquifer sediments of Bangladesh: Implications for widespread microbial contamination of groundwater, *Water Resour. Res.*, *49*, 3897–3911, doi:10.1002/wrcr.20289.

1. Introduction

[2] The microbiological quality of groundwater is often better and more stable than that of surface water [*Katayama*, 2008]. As a result, untreated groundwater is a common source of drinking water in developing countries and also among many communities in developed countries. Growing evidence of widespread microbial contamination of groundwater, however, has prompted concern about the human health risks associated with the consumption of untreated groundwater. In the passive surveillance of 11,000 private water supplies in England, 32% of sites tested positive at least once for *E. coli* [*Richardson et al*., 2009] and 10% of 144 private water supplies surveyed in Netherlands tested positive for *E. coli* or intestinal enterococci [*Schets et al*., 2005]. In the United States, consumption of untreated groundwater water has been associated with increased risk of infection by *E. coli* O157:H7 [*Slutsker et al*., 1998], and outbreaks of this strain have been linked to contaminated groundwater [*Olsen et al*., 2002; *Bopp et al*., 2003]. In the setting that is the focus of this study, monthly monitoring of over 100 shallow (<36 m deep) tubewells in rural Bangladesh has shown that between 30 and 70% of wells are contaminated with detectable levels of *E. coli*, with contamination in some wells reaching levels greater than 100 colony forming units (CFU)/100 mL [*van Geen et al*., 2011]. Within a subset of these wells, the frequency of *E. coli* detection has been shown to be associated with increased likelihood of contamination by pathogenic *Shigella*, *E. coli*, and *Vibrio* [*Ferguson et al*., 2012].

[3] The three major processes that control microbial transport in aquifer systems are (i) the physical transport processes of advection and hydrodynamic dispersion, (ii)

[1]Department of Earth and Environmental Engineering, Columbia University, New York City, New York, USA.
[2]Department of Environmental Sciences, Barnard College, New York City, New York, USA.
[3]Department of Civil Engineering and Engineering Mechanics, Columbia University, New York City, New York, USA.
[4]Department of Geology, University of Dhaka, Dhaka, Bangladesh.
[5]Lamont-Doherty Earth Observatory of Columbia University, Palisades, New York, USA.

Corresponding author: P. J. Culligan, Room 626, SW Mudd Building, 500 West 120th St., New York, NY 10027, USA. (pjc2104@columbia.edu)

0043-1397/13/10.1002/wrcr.20289

interactions between microbes and the aquifer's solid phase, and (iii) microbe decay [*Tufenkji*, 2007]. Traditional approaches to modeling microbial transport during saturated flow involve the advection-dispersion equation coupled with terms that describe attachment to and detachment from the solid phase during transport as a result of physicochemical interactions. Microbe attachment is assumed to be either irreversible, in which case microbes are permanently filtered from the mobile liquid phase, or reversible, in which case microbes can reenter the flowing liquid. Under classical colloid filtration theory (CFT), microbes are considered to irreversibly attach to the solid phase, and the rate of attachment is related to the probability of a collision with the collector surface, which is derived mechanistically from a sphere and shell model [*Happel*, 1958] and modified by a collision efficiency α, defined as the probability of the particle being captured [*Yao et al*., 1971; *Rajagopalan and Tien*, 1976; *Logan et al*., 1995]. This approach has proven successful under conditions favorable for microbial attachment; however, CFT deviates from observations in many situations of environmental relevance where an energy barrier to microbial attachment exists due to low ionic strength in the liquid phase or heterogeneity in surface charges [*Johnson et al*., 2007a; *Tufenkji and Elimelech*, 2005]. Recent evidence from micromodel studies using particle-tracking numerical models or direct visualization of microsphere surrogates show that under unfavorable electrostatic attachment conditions, particle-collector attachment mechanisms include wedging in grain-to-grain contact points [*Johnson et al*., 2007b; *Li et al*., 2006], capture by surface asperities [*Yoon et al*., 2006], trapping in hydrodynamic dead zones [*Li et al*., 2010], and weak surface attachment in a secondary energy minima [*Tufenkji and Elimelech*, 2005; *Redman et al*., 2004]. Few experiments to date have focused on determining whether these attachment mechanisms are applicable to bacterial transport under field-like conditions.

[4] Attachment rates for bacteria have been inferred under various conditions from aquifer-scale forced gradient and natural gradient tracer tests [*Harvey et al*., 1989; *Bales et al*., 1997; *Knappett et al*., 2012] or centimeter-scale column experiments [*Harvey et al*., 1993; *Litton and Olson*, 1993; *Fitzpatrick and Spielman*, 1973] using stained bacteria or latex microspheres with size and surface properties that are similar to bacteria. Recent reviews have focused on the apparent discrepancy between rates of bacterial transport measured in laboratory columns versus field transport experiments, generally manifested as an apparent decrease in measured attachment rates with increasing scale of the experiment [*Foppen and Schijven*, 2006; *Dong et al*., 2006; *Pang et al*., 2008; *Scheibe et al*., 2011]. One proposed explanation is that there is a subpopulation of less adhesive bacteria that are not easily detected at the scale of a typical column experiment [*Bolster et al*., 2000]. The transport of bacteria, and other colloidal-sized particles, with subpopulations has been modeled using a modification of CFT incorporating two independent values for the collision efficiency [*Simoni et al*., 1998; *Foppen et al*., 2007a], a bimodal distribution [*Tufenkji and Elimelech*, 2004], and various other probability distributions [*Brown and Abramson*, 2006; *Abramson and Brown*, 2007]. One of the major shortcomings of using CFT under unfavorable attachment conditions is the failure to account for bacterial detachment and reentrainment into the liquid phase [*Johnson et al*., 2007a; *Tufenkji*, 2007]. To account for subsequent detachment, dual-deposition kinetic models assume separate modes of bacteria-surface interaction with unique attachment and detachment rates to account for electrostatic attachment independently from other processes such as straining in dead-end pore spaces [*Bradford et al*., 2005; *Foppen et al*., 2007b], trapping at grain-to-grain contacts [*Yoon et al*., 2006; *Basha and Culligan*, 2010], or hydrodynamic retention in flow stagnation zones [*Johnson et al*., 2007b].

[5] In a dual-deposition mode kinetic model, the advection-dispersion equation, simplified to one dimension, for a saturated, homogeneous porous medium with two adsorption sites is expressed as [*Schijven et al*., 2002]

$$\frac{\partial c}{\partial t}+\frac{\rho_b}{\theta}\frac{\partial s_r}{\partial t}+\frac{\rho_b}{\theta}\frac{\partial s_i}{\partial t}=D\frac{\partial^2 c}{\partial z^2}-u\frac{\partial c}{\partial z}-\mu_c c-\mu_r\frac{\rho_b}{\theta}s_r-\mu_i\frac{\rho_b}{\theta}s_i, \tag{1}$$

where c is the mass concentration of bacteria in the liquid phase, s_r is the reversibly adsorbed solid-phase concentration of bacteria (in units of mass of particles per mass of solid phase), s_i is the irreversibly adsorbed solid-phase concentration, t is time, ρ_b is the bulk density of the solid phase, θ is the porosity of the medium, D is the hydrodynamic dispersion coefficient, u is the pore (or interstitial) velocity, z is distance from the inlet, μ_c is the decay (or die-off) rate for the liquid-phase bacteria, and μ_r and μ_i are decay rates for the solid phase reversibly and irreversibly attached bacteria, respectively.

[6] The rates of transfer of bacteria to the solid phase (terms 2 and 3 of equation (1)) can be expressed as

$$\frac{\rho_b}{\theta}\frac{\partial s_r}{\partial t}=k_a c-\frac{\rho_b}{\theta}k_d s_r-\mu_r\frac{\rho_b}{\theta}s_r, \tag{2}$$

$$\frac{\rho_b}{\theta}\frac{\partial s_i}{\partial t}=k_i c-\mu_i\frac{\rho_b}{\theta}s_i, \tag{3}$$

where k_a is the reversible attachment rate, k_d is the reversible detachment rate, and k_i is the irreversible attachment rate.

[7] Given the multitude of properties known to influence the rates of bacterial attachment and detachment under highly uniform laboratory conditions, relatively few studies have been able to determine which of these parameters are most influential in actual field sediments. The present study applies treatments to field sediments to examine the effects of sediment layering, grain size heterogeneity, and geochemical heterogeneity on *E. coli* transport in saturated aquifer material. The experimental data are fit to a dual-population model with two sites that account for reversible and irreversible bacterial attachment. Parameters extracted from model fitting are used to simulate bacterial transport in an aquifer system in order to explore how dual-population transport might contribute to the observed, widespread microbial contamination of groundwater.

2. Methods

2.1. Collection of Sediment Cores and Drill Cuttings

[8] Intact cores and disturbed sediment samples were obtained while installing several monitoring wells in Matlab, Bangladesh (23.37233°N, 90.64438°E) in August 2008. Drilling logs indicate a 3–6 m thick silty-clay layer capping a fine gray sand aquifer, which extends to 15–25 m depth and is tapped by the majority of shallow tubewells in the area that were monitored for *E. coli* and/or microbial pathogens [*Ferguson et al*., 2012; *van Geen et al*., 2011]. The site stratigraphy, consisting of fine-grained sand units separated by relatively thin clay and silt layers, is typical of the estuarine plain of the Meghna River [*Khan and Islam*, 2008].

[9] The sediment cores were recovered using the local reverse circulation drilling method. Drilling was stopped every 0.9 m (3 ft), and a soil core sampler (AMS, American Falls, Idaho) was inserted into the drilling pipe and driven at least 0.3 m (1 ft) past the bottom of the hole. The soil was recovered into a 1.9 cm (3/4 in) OD × 30.5 cm (12 in) long, butyrate plastic core liner (Forestry Suppliers, Jackson, MS). The sampled cores were capped, stored immediately at 4°C, and frozen within 24 h for return to the Columbia University laboratories in the United States. At regular depth intervals, aquifer sediment was also recovered from the cuttings produced during drilling. The drill cuttings were collected in a bucket, which was then poured onto the ground to drain excess water. The remaining wet material was sealed in a zip-lock bag and stored under ambient conditions, also for return to the Columbia University laboratories.

2.2. Sediment Treatments

[10] The aquifer sediments used in the experiments included the sediment cores recovered from the field site that were frozen and returned to the laboratory for testing (referred to as SC), dried drill cuttings (referred to as DC, or DCE for extended duration experiments), and washed drill cuttings (referred to as WC). Upon return to the laboratory, all drill cuttings were dried at 100°C for 12 h. Washed cuttings were then further prepared by soaking sediment in 12 *N* HCl for 24 h, rinsing with deionized water until the pH was circumneutral, and then redrying at 100°C for 12 h. Prior to each experiment, the frozen cores were thawed for 12 h at 4°C, then 12 h at room temperature.

Table 1. Sources, Treatments, and Grain Size Information for Sediments

Sediment	Depth (m)	Treatment	D_{50} (mm)	D_{10} (mm)	U_i
DC	15.2	Dried, repacked	0.169	0.090	2.07
DCE/1	15.2–18.3	Dried, repacked	0.183	0.130	1.52
DCE/2	7.6–10.6	Dried, repacked	0.118	0.070	1.97
WC	15.2	Acid-washed, repacked	0.179	0.127	1.53
SC-3.5-1	9.1	Frozen, thawed	0.093		
SC-3.5-2	4.6	Frozen, thawed	0.162	0.079	2.27
SC-3.5-3	9.1	Frozen, thawed	0.103	0.066	1.60
SC-3.5-4	4.6	Frozen, thawed	0.297	0.104	3.21
SC-20-5	7.6	Frozen, thawed	0.085		
SC-20-6	9.1	Frozen, thawed	0.159	0.075	2.32

[11] The grain size distributions of the sediments used for the column experiments were obtained by grain-size analyses following the ASTM D 422 protocols described by *Liu and Evett* [2003]. Sediment sources and depth are summarized in Table 1, along with the values for average grain size, D_{50}; the grain diameter for the smallest 10% of particle mass, D_{10}; and the coefficient of uniformity, U_i. The grain size distributions for the intact sediment cores were obtained in the same manner after the sections were dried at the end of each column experiment. X-ray images (Figure 1) of two cored sediments were obtained with a Dynarad 150 (JCF Engineering, Inc., CO) using an exposure time of 30 s at 60 kV and 5 mA.

2.3. Preparation of Test Solutions

[12] Artificial groundwater (AGW) was made at ionic strengths of 3.5 and 20 mM with KCl and was designed to encompass the range of ionic strength observed in ponds contaminated with fecal bacteria, which are believed to be a source of aquifer contamination [*Knappett et al*., 2012], at the field site in Bangladesh where the cores were collected. Specifically, an ionic strength of 3.5 mM is approximately representative of pond conditions during the monsoon season, whereas higher ionic strengths of approximately 20 mM are observed during the dry season [*van Geen et al*., 2011]. Contaminated AGW consisted of a KCl solution amended with 20 mg L^{-1} of bromide (as KBr) to act as an inorganic tracer. The KCl concentration for contaminated AGW was adjusted to compensate for the bromide addition so that the solution electrical conductivity was within ±20 μS/cm of the clean AGW. Contaminated AGW also contained nontoxigenic, nalidixic acid-resistant *E. coli* (ATCC 700609, strain CN13) at approximate concentrations of 10^6 CFU/mL. This strain of *E. coli* is rod shaped and approximately 1 μm long by 0.25 μm in diameter. Bacteria for each laboratory column experiment were cultured from 100 μL of frozen stock in 5 mL of Luria Broth with nalidixic acid for 12 h at 37∘C. Cultured bacteria were then washed three times in AGW solution and resuspended in AGW 8 h prior to the start of a test.

2.4. Preparation of Columns

[13] All column experiments were performed in the butyrate plastic core liners (Forestry Suppliers, Jackson, MS) that were used to collect the sediment cores. The SC experiments used columns that ranged from 9 to 12 cm in length; all others used 11–12 cm columns. Custom Teflon end caps were made for the column experiments, and a fine stainless steel mesh screen was placed at each end of the column. For the SC experiments, a 12 cm long section of the 35 cm core obtained from the field that was free of visible void spaces and air bubbles was selected for testing. For the DC and WC experiments, the columns were packed dry with either the dried drill cuttings or the washed and redried drill cuttings. Columns were vibrated and tamped every 2 cm and then saturated slowly from the bottom upward using the clean AGW.

2.5. Column Test Protocol

[14] All column experiments were conducted under downward flow at a constant Darcy velocity between 2.9 and 3.6 m/day that was maintained with a peristaltic pump (Gilson MiniPuls, Middleton, WI). The test protocol

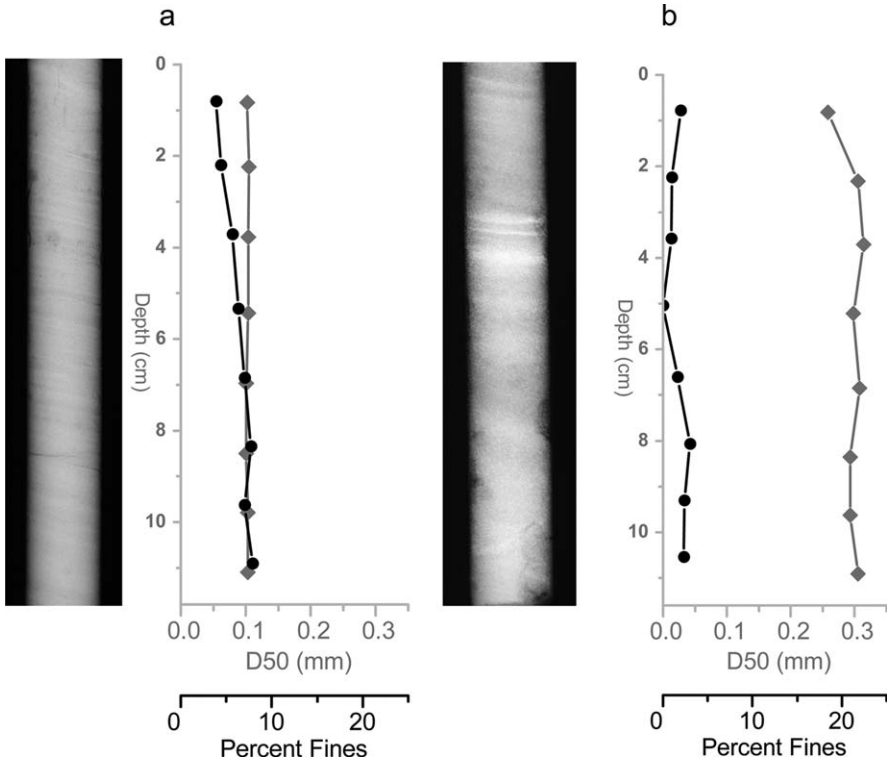

Figure 1. X-ray images of cores (a) SC-3.5-3 and (b) SC-3.5-4 shown alongside profiles of average grain size (light gray diamonds) and percent fine material (mass basis) with $D_{50} < 0.063$ mm (dark circles).

consisted of an initial purge with approximately 10 pore volumes (PV) of the clean AGW, followed by a 15 PV injection of contaminated AGW, then a further 10 PV injection of the clean AGW. In order to assess possible changes that occurred in the retained particle concentrations with time, extended duration column experiments were performed using a similar protocol except that the final purge using clean solution was increased up to 180 PV. Column-effluent samples were collected with a fraction collector (LKB-Bromma, Sweden). Samples of the clean and contaminated AGW were also taken before and after each experiment. A total of 20 column experiments were performed, comprising duplicate experiments with dried drill cuttings (DC) and washed drill cuttings (WC) at two ionic strengths, two triplicate extended duration experiments, and six individual experiments with intact sediment cores.

2.6. E. coli and Bromide Determinations

[15] Immediately following a column experiment, the collected effluent samples were analyzed for *E. coli* using the IDEXX Quanti-Tray 2000 method using Colilert media according to the manufacturer's protocols (IDEXX, Westbrook, ME). Samples were mixed with deionized water to obtain appropriate dilutions. The number of positive total coliform and positive *E. coli* wells were counted visually and converted to a most probable number (MPN) estimate in CFU/100 mL. Bromide tracer concentrations were measured by ion chromatography and normalized concentrations were modeled using CXT-FIT/Excel v. 2.0 [*Toride et al.*, 1995] to obtain estimates of pore velocity and longitudinal dispersivity.

2.7. Extraction of Retained Bacteria

[16] Profiles of retained bacteria were determined at 1.5 cm increments for each column at the end of each experiment. The columns were split lengthwise using a sterile knife, and 1.5 cm sections were removed using a sterile spatula. Twenty milliliters of sterile deionized water was added to the sediment extracted from each column section, which was then vortexed for 5 s and placed on an orbital shaker at 37°C for 30 min. Aliquots of the supernatant were then immediately analyzed in the same manner as the column effluent samples. The sediment from the SC experiments was also dried, weighed, and then analyzed for grain size distribution.

2.8. E. coli Decay Experiment

[17] The decay rate of *E. coli* was measured in microcosm experiments over a period of 12 days. Five grams of dried drill cuttings was mixed with 10 mL of 3.5 m*M* AGW with a known concentration of *E. coli* in 15 mL polypropylene test tubes. The tubes were inverted several times, placed on an orbital shaker, and gently shaken for 30 min. The excess supernatant was removed and analyzed for *E. coli* to determine initial attached and planktonic concentrations. The tubes were then kept in the dark at room temperature (21°C) without shaking. A total of 15 tubes were prepared in this manner, providing for five groups of triplicate samples.

[18] On days 1, 2, 4, and 7, one group of tubes was sacrificed to measure attached bacteria and the other remaining

tubes were analyzed for planktonic bacteria. An additional group of control tubes containing only AGW and *E. coli* was used to measure liquid-phase bacterial decay rate. The methods for determining *E. coli* concentrations were identical to those used in the column experiments.

[19] Any observed difference in the measured liquid-only versus the measured liquid-plus-sediment rate of decrease in concentration can be interpreted in two ways: (i) the liquid decay rate increased due to interaction between the bacteria and the sediment or (ii) the increased decay rate is due to attachment of bacteria to the solid phase. In calculating the solid-phase concentrations, the second explanation was assumed, and the solid-phase bacteria concentration was corrected for subsequent attachment of bacteria from the liquid phase. The correction was made by reducing the number of bacteria estimated to have been extracted from the sediment by the number of bacteria that disappeared from the liquid phase at each time step, after accounting for the bacteria that decayed in the liquid phase (based on the average decay rate from the liquid-only control tubes). Therefore, the corrected number of bacteria attached to the solid phase is given by

$$N_{\text{corrected}} = N_{\text{extracted}} - \sum_{n=2}^{m} V_l \left[c_{(n)} - c_{(n-1)} - \left(\frac{c_{(n)} + c_{(n-1)}}{2} \right) \left(1 - 10^{-\mu_c \Delta t} \right) \right], \quad (4)$$

where N is the number of bacteria, V_l is the liquid volume in the tube, c_l is the liquid concentration measured in the tube, Δt is the elapsed time between measurements, m is the total number of measurements, and μ_c is the liquid decay rate measured for the liquid only control tubes.

[20] First-order decay rates were determined by fitting to the following equation:

$$c = c_0 \cdot 10^{-\mu_c t}, \quad (5)$$

where c is the bacteria concentration at time t, c_0 is the initial concentration at the beginning of the experiment, and μ_c is the liquid-phase decay rate expressed in units of $\log_{10}$ per day.

2.9. Numerical Modeling

[21] In order to simplify the units of the transport equations for numerical modeling, a nondimensionalization scheme similar to that of *Basha and Culligan* [2010] was invoked by introducing the following dimensionless groups:

$$C = \frac{c}{c_0}, \quad S = \frac{\rho_b}{\theta} \frac{s}{c_0}, \quad Z = \frac{z}{L}, \quad T = \frac{u}{L} t, \quad v = \frac{D}{uL}, \quad K = \frac{L}{u} k, \quad M = \frac{L}{u} \mu. \quad (6)$$

[22] The nondimensionized advection-dispersion equation becomes

$$\frac{\partial C}{\partial T} + \frac{\partial S_r}{\partial T} + \frac{\partial S_i}{\partial T} = v \frac{\partial^2 C}{\partial Z^2} - \frac{\partial C}{\partial Z} - M_c C - M_r S_r - M_i S_i, \quad (7)$$

and the attachment rates (equations (2) and (3)) are transformed as follows:

$$\frac{\partial S_r}{\partial T} = K_a C - K_d S_r - M_r S_r, \quad (8)$$

$$\frac{\partial S_i}{\partial T} = K_i C - M_i S_i. \quad (9)$$

[23] Equations (7)–(9) were solved simultaneously using a finite difference algorithm that is centered in time and space. The finite difference model was developed using MATLAB software version R2010b (Mathworks, Inc., Natick, MA) and included a function for importing observed column test data for comparison to model values. Fitting of model parameter values to the observed experimental data was done using the MATLAB fmincon built-in optimization routine with a weighted least-squares objective function. Since the objective function included both temporally and spatially varying datasets, weights were applied to each data point such that the observed value was divided by the product of the variance and the number of data points within the data set [*Simunek and Hopmans*, 2002]. The adjusted R^2 statistic was computed to compare goodness of fit between different experiments and Akaike's Information Criterion (AIC) was computed to compare models with different numbers of fitting parameters [*Akaike*, 1974].

2.10. Parameter Estimation

[24] Applying equations (7)–(9) for two populations would require fitting nine rate parameters in addition to the proportion of the second population, w. In order to reduce the number of fitting parameters, the decay rates (μ_c, μ_r, and μ_i) were measured independently in the earlier described microcosm experiments and assumed to be constant, while the reversible attachment and detachment rates were assumed to be the same for both populations ($k_{a(1)} = k_{a(2)}$ and $k_{d(1)} = k_{d(2)}$) [*Basha and Culligan*, 2010].

[25] To determine whether the experimental results could be modeled with simplified versions of equation (7), the column data were fit in stages. First, a single forward attachment rate model—analogous to CFT–was used to fit the experimental data, then data were fit with a single-population dual-deposition mode (reversible/irreversible) model, and finally the two-population dual-deposition model was used. The experimental data were also used to evaluate a single-population, two-reversible-sites model (sometimes referred to as a "fast/slow" reversible attachment model), in which equation (9) is modified by adding independent reversible attachment and detachment rates. However, the fast/slow model did not result in an improvement over the two-population model for any of the experimental conditions investigated during this study, and thus results from this model are not presented here.

[26] In most experiments, a small peak in breakthrough concentration was observed within the first PV following the switch from contaminated AGW back to clean AGW. These observed peaks are not included in the figures

Table 2. Porosity (θ) and Longitudinal Dispersivity (λ_L) Determined From Bromide Tracer

Column	Sediment	θ	SE	λ_L (cm)	SE (cm)	R^2
DC-3.5a	Drill cuttings	0.39	0.03	0.326	0.425	0.76
DC-3.5b		0.41	0.00	0.663	0.000	0.85
DC-20a		0.37	0.01	0.328	0.124	0.95
DC-20b		0.35	0.03	0.433	0.475	0.87
WC-3.5a	Washed drill cuttings	0.42	0.02	0.158	0.171	0.98
WC-3.5b		0.45	0.03	0.237	0.257	0.87
WC-20a		0.40	0.01	0.190	0.119	0.96
WC-20b		0.39	0.03	0.194	0.158	0.97
SC-3.5-1	Sediment cores	0.42	0.11	0.516	1.438	0.91
SC-3.5-2		0.36	0.02	0.267	0.188	0.95
SC-3.5-3		0.41	0.01	0.261	0.074	0.96
SC-3.5-4		0.43	0.02	0.264	0.229	0.93
SC-20-5		0.41	0.03	0.470	0.172	0.98
SC-20-6		0.37	0.03	0.269	0.315	0.90
DCE-3.5a	Drill cuttings	0.40	0.03	0.257	0.238	0.93
DCE-3.5a		0.36	0.01	0.127	0.161	0.99

presented in this paper, nor were they considered in the model fits. To further investigate these peaks, an experiment (data not shown) was performed in which the valve was switched between the contaminated solution and another tube immersed in, and primed with, the exact same solution to determine whether the peak was caused by a pressure pulse induced by the switching process. Later, the valve was switched back to the original line, which was now immersed in the clean solution. A peak was observed only during the switch back to clean AGW, indicating that small differences in ionic strength, or the presence or absence of the bromide anion, are the cause of the peaks.

3. Results

3.1. Sediment Cores

[27] The intact sediment cores had average grain diameters (D_{50}) that ranged from 0.085 mm to as high as 0.297 mm (Table 1) and all had uniformity coefficients less than 3, except for SC-3.5-4 ($U_i = 3.21$). In the X-ray images, Core SC-3.5-3 (Figure 1a) contained bands of fine-grained sediment, which appear lighter in the images, separated by narrower bands of coarser material (SC refers to sediment core, 3.5 to the ionic strength, and 3 to the replicate). Core SC-3.5-3 was obtained from a depth of 9.1 m and had an average grain size of 0.103 mm. X-ray images of Core SC-3.5-4 (Figure 1b) indicated the presence of bands of finer material between a depth of 3 and 4 cm from the inlet. Of the two cores with X-ray images, SC-3.5-4 had more prominent lighter-colored layers of fine material, which helps explain the larger coefficient of uniformity. SC-3.5-4 was obtained from a depth of 4.6 m and had an average grain size of 0.297 mm.

[28] A total of four SC columns were tested at an ionic strength of 3.5 mM while two were tested at 20 mM. The porosities of the SC columns were between 0.36 and 0.43 and the longitudinal dispersivities were 0.261–0.516 cm (Table 2). The normalized breakthrough concentrations for SC-3.5-2 and SC-3.5-4 (Figure 2) were highest in this series ($C = 0.02$ rising to 0.04 and 0.06, respectively). It should be noted that the relative error of the MPN estimate is highest at both the low and high end of the analytical range; therefore, depending on the dilution factor used, error bars from certain experiments appear larger or smaller than others. The grain size profiles indicate that these two columns had higher average grain diameters and lower percentages of fine material than the other two experiments in this series. Cores SC-3.5-1 and SC-3.5-3 had very low normalized breakthrough concentrations, beginning at 0.005 and rising to 0.01. All of the low ionic strength cores exhibited some degree of bacterial detachment throughout the duration of the experiment. The mass recovery, estimated by integrating the area under the breakthrough and retained bacteria curves and dividing by the number of bacteria introduced, was 79–94% for experiments SC-3.5-1 through −3, but was lower for SC-3.5-4 (62%). The retained bacteria profile of Core SC-3.5-2 has a peak near the outlet, and the grain size data shows a small decrease in average diameter in the same region. Core SC-3.5-3 has a peak near the dimensionless depth of 0.3 that does not appear to coincide with any change in the grain size profile or any noticeable changes in the X-ray image (Figure 1).

[29] SC-20-5 essentially had no breakthrough and no subsequent detachment, whereas SC-20-6 had a normalized concentration of 0.04 increasing to 0.07 and remaining above 0.01 following the switch back to a noncontaminated inlet solution. Both of these columns had hyperexponential-retained bacteria profiles, yet both also had high levels of fine material (20–25%) in the first 25% of their length, followed by a decrease in fines in through the rest of the core, which might have contributed to the higher concentrations observed in the first section.

[30] The single-population model was sufficient to fit all of the low ionic strength experimental results, except for SC-3.5-4, for which the AIC decreased slightly with the addition of a small (14%) population of bacteria with a lower irreversible attachment rate (Table 3). SC-3.5-4 had the largest average grain size ($D_{50} = 0.297$ mm) of all the column experiments and had less than 5% fine material throughout. The low ionic strength sediment cores had reversible attachment rates as low as 2.64 h^{-1} for SC-3.5-4 and as high as 9.18 h^{-1} for SC-3.5-3. The detachment rates were between 0.17 and 0.94 h^{-1}. The irreversible attachment rates were higher than the reversible rates, ranging between 5.70 and 13.14 h^{-1} for the single-population fits (SC-3.5-1 to −3) and up to the maximum value of 60 h^{-1} allowed by the software for the first population in SC-3.5-4. The two high ionic strength cores (SC-20-5 and SC-20-6) had very different reversible attachment rates (18.12 versus 2.64 h^{-1}) but similar detachment rates, and both had a high irreversible attachment rate (for the first population in the case of SC-20-6). SC-20-6 had a better fit with the two-population model (AIC reduced from −71.5 to −32.8), but this may have been influenced by the sudden transition in the amount of fine material within the first two columns sections, which decreased from 20 to 5% over the normalized length of 0.25 from the inlet.

3.2. Repacked Drill Cuttings

[31] The unwashed drill cuttings, DC, were obtained from a depth of 15.2 m and had an average grain size of 0.169 mm and uniformity coefficients of less than 3 (Table 1). The grain size of the washed cuttings, WC, was slightly

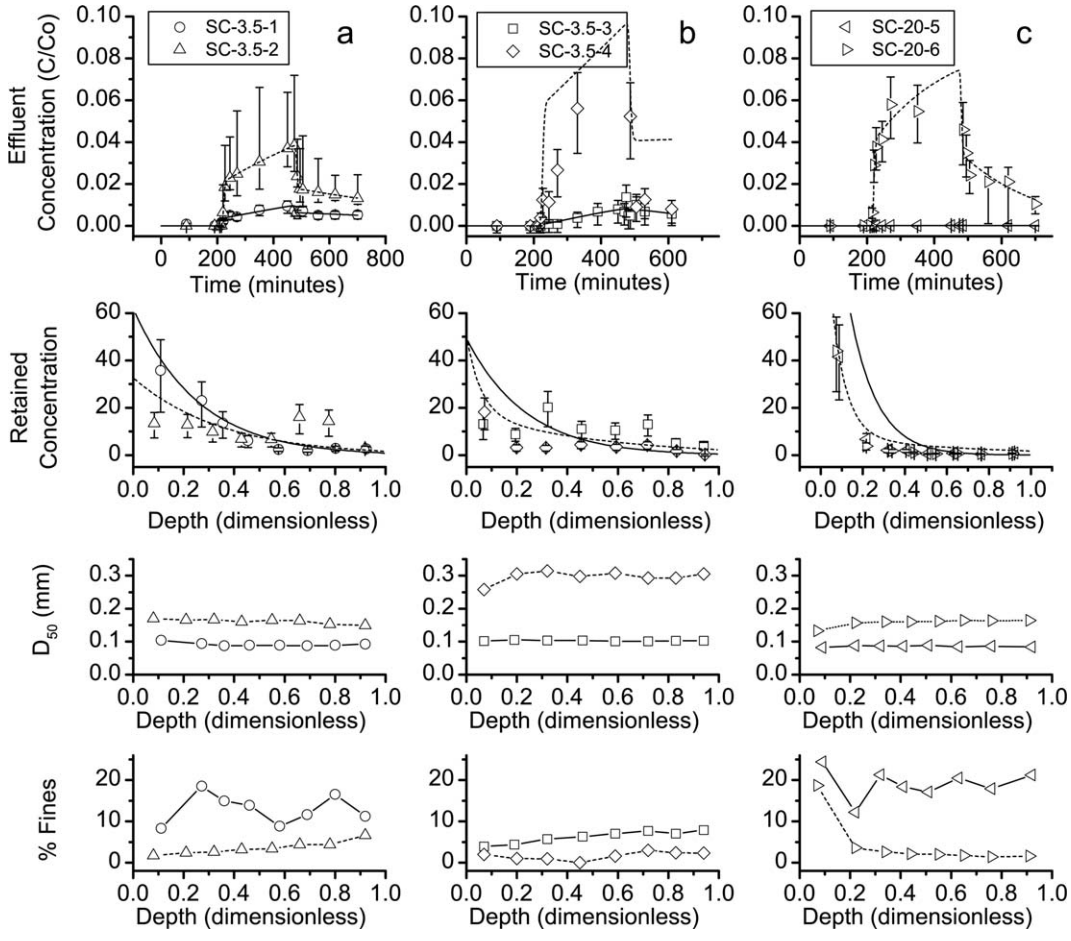

Figure 2. Breakthrough curves and retained bacteria profiles for the experiments with preserved sediment cores. (a and b) The results from two experiments conducted with 3.5 mM ionic strength solution, followed below by the retained concentration profiles, the average grain size, and the percent (mass basis) of fine material with $D_{50} < 0.063$ mm. (c) The high ionic strength (20 mM) experiments. Error bars represent the upper and lower 95% confidence interval.

Table 3. Fitted Parameters for One-Population and Two-Population Models

		Single Population					Two Populations						
Column[a]	Recovery (%)	k_a (h^{-1})	k_d (h^{-1})	k_i (h^{-1})	Adj R^2	AIC	k_a (h^{-1})	k_d (h^{-1})	k_{i1} (h^{-1})	k_{i2} (h^{-1})	w	Adj R^2	AIC
DC-3.5a	93	6.84	0.17	2.58	0.75	−33.8	6.84	0.17	2.58		0.00	0.75	−33.8
DC-3.5b	112	3.48	1.07	4.20	0.96	−48.1	2.88	0.59	7.98	0.00	0.24	0.97	−58.8
DC-20a	103	4.56	0.21	7.80	0.93	−61.2	4.56	0.21	7.80		0.00	0.93	−61.2
DC-20b	79	3.66	0.30	11.46	0.86	−65.4	3.66	0.30	11.46		0.00	0.86	−65.4
WC-3.5a[b]	*93*	*0.00*	*0.00*	*1.98*	*0.58*	*45.4*	*0.00*	*0.00*	*33.12*	*0.30*	*0.41*	*0.93*	*1.4*
WC-3.5b	*97*	*0.00*	*0.00*	*1.26*	*0.66*	*39.8*	*0.00*	*0.00*	*24.66*	*0.48*	*0.22*	*0.95*	*−6.8*
WC-20a	67	6.18	0.24	9.06	0.43	−50.0	6.18	0.24	9.06		0.00	0.43	−50.0
WC-20b	69	5.88	0.14	7.62	0.73	−65.7	5.88	0.14	7.62		0.00	0.73	−65.7
SC-3.5-1	92	8.52	0.25	13.14	0.96	−158.2	8.52	0.25	13.14		0.00	0.96	−158.2
SC-3.5-2	79	4.26	0.17	6.96	0.67	−46.6	4.26	0.17	6.96		0.00	0.69	−47.7
SC-3.5-3	94	9.18	0.89	11.70	0.50	−79.8	9.18	0.89	11.70		0.07	0.50	−79.8
SC-3.5-4	*62*	*2.64*	*1.19*	*5.70*	*0.72*	*−22.3*	*2.46*	*0.94*	*60.00*	*5.16*	*0.14*	*0.77*	*−27.0*
SC-20-5	48	18.12	0.38	42.54	0.83	−204.9	17.82	0.40	42.96		0.00	0.83	−209.8
SC-20-6	*58*	*2.64*	*0.50*	*7.86*	*0.72*	*−32.8*	*2.64*	*0.41*	*60.00*	*5.16*	*0.52*	*0.95*	*−71.5*
DCE-3.5-1a	*93*	*0.00*	*0.00*	*2.10*	*0.86*	*14.0*	*0.00*	*0.00*	*19.26*	*1.44*	*0.14*	*0.94*	*−6.7*
DCE-3.5-1b	*90*	*0.54*	*0.59*	*3.36*	*0.92*	*−27.1*	*0.60*	*0.24*	*7.80*	*0.00*	*0.66*	*0.96*	*−51.5*
DCE-3.5-1c	*80*	*1.44*	*0.14*	*2.76*	*0.88*	*−55.4*	*2.10*	*0.06*	*5.46*	*0.00*	*0.38*	*0.92*	*−70.1*
DCE-3.5-2a	62	2.40	1.33	5.46	0.74	−6.9	2.40	1.32	5.46		0.00	0.74	−6.9
DCE-3.5-2b	*54*	*2.94*	*0.10*	*2.82*	*0.78*	*−28.2*	*6.00*	*0.12*	*60.00*	*0.00*	*0.09*	*0.87*	*−42.5*
DCE-3.5-2c	71	4.98	0.08	1.68	0.97	−96.7	5.28	0.06	2.34	0.00	0.37	0.98	−97.9

[a]Columns are coded as follows: DC = drill cuttings, WC = washed drill cuttings, SC = sediment core. DCE were extended duration experiments using drill cuttings in which replicate columns were stopped at different times. The number following the dash is the ionic strength (3.5 or 20 mM).

[b]The values in italics signify experiments in which the two-population model was favored, based on a decrease in the AIC.

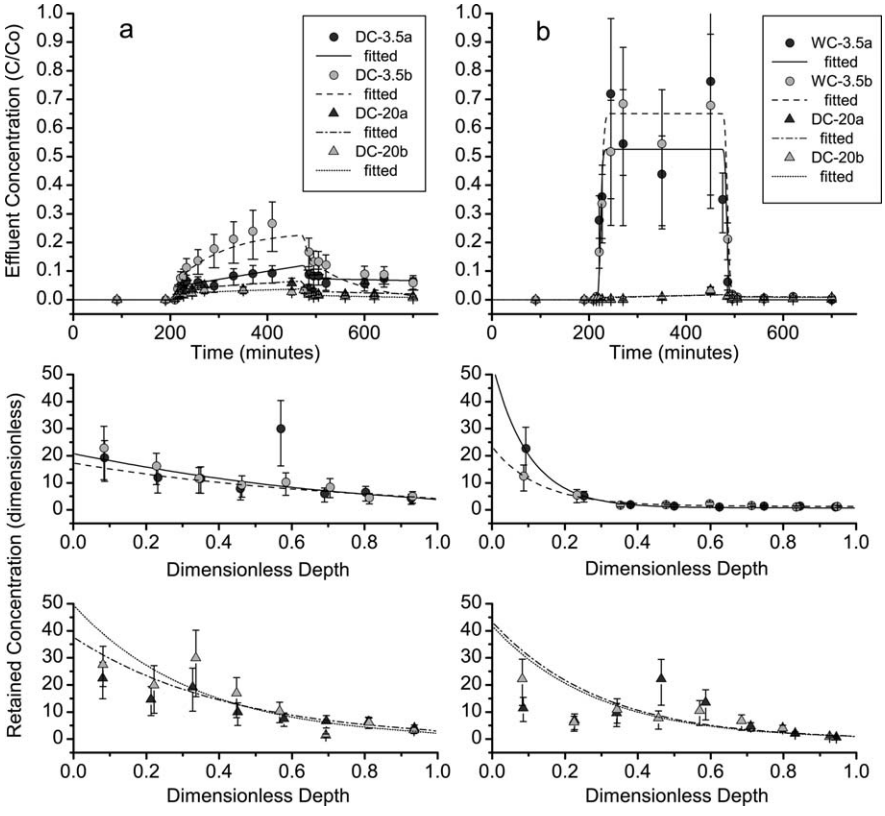

Figure 3. Breakthrough curves (top) and retained bacteria concentrations (separated into two lower plots for clarity) for (a) unwashed drill cuttings and (b) washed drill cuttings. Each breakthrough curve (Figures 3a and 3b) contains the results of four experiments: two replicates conducted at two ionic strengths. Error bars represent the upper and lower 95% confidence interval.

higher at 0.179 mm. The DC columns had porosities between 0.35 and 0.41 and longitudinal dispersivities between 0.326 and 0.663 cm.

[32] The low ionic strength experiments (3.5 mM) begin with an initial normalized breakthrough concentration of approximately 0.05 and 0.10 (Figure 3a, circles); then normalized concentrations rose to 0.10 and 0.25 for columns DC-3.5a and DC-3.5b, respectively. Detachment of bacteria continued following the switch back to clean groundwater with normalized concentrations remaining at 0.10 for both columns for the rest of the experiment. The high ionic strength experiments (Figure 3a, triangles) had a relatively flat breakthrough of 0.05 and very little detachment following the switch back to clean solution. The total mass recovery for bacteria, determined by integrating the area under the observed breakthrough and retained curves, was between 79 and 112% for the unwashed cuttings.

[33] The modeling of the DC experiments did not improve from applying the two-population model; therefore, the one-population model fit is shown in Figure 4. The reversible attachment rates for high and low ionic strength were between 3.48 to 6.84 h^{-1}. The detachment rates were between 0.17 and 1.07 h^{-1}. The irreversible attachment rates were 2.58 and 4.20 h^{-1} for the 3.5 mM and 7.8 and 11.46 h^{-1} for the 20 mM experiments, respectively.

[34] The WC experiments conducted at low ionic strength had normalized breakthrough concentrations between 0.5 and 0.8 (Figure 3b, circles), which did not increase over the contamination phase of the experiment. The high ionic strength experiments had very little breakthrough initially (Figure 3b, triangles) and then increased slightly to 0.03 by the end of the experiment. Detachment was negligible for washed cuttings at both ionic strengths. Mass recovery was 93–97% for the low ionic strength experiments and 67–69% for the high ionic strength experiments.

[35] The results from WC experiments at low ionic strength were fit poorly with the one-population model (adjusted $R^2 = 0.60$ and 0.67) due to the hyperexponential shape of the retained particle profiles. Adding a second population resulted in an improved fit (AIC reduced by 44 and 46, respectively). In this model, the reversible attachment and detachment rates were zero, and the main population had high irreversible attachment rates of 33.12 and 24.66 h^{-1} while a minor population (30 and 48%) had very low irreversible attachment rates of 0.41 and 0.22 h^{-1}. This model was able to fit the steep decrease in retained bacteria close to the column inlet. The high ionic strength washed cuttings were fit poorly due to the dual peaks in retained bacteria observed at both the inlet and midway through the column. None of the models described in this paper could fit these secondary peaks.

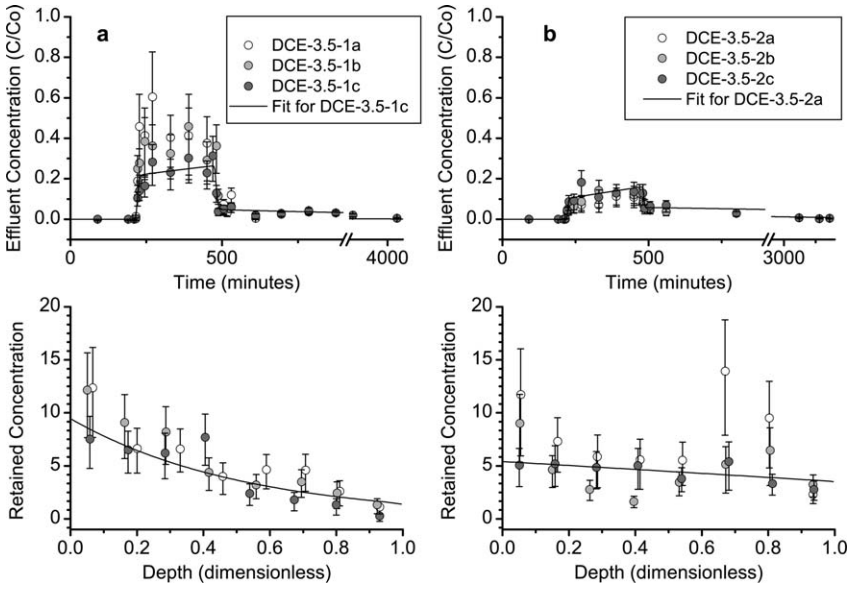

Figure 4. Breakthrough curves and retained bacteria profiles for the two extended duration column experiments conducted at 3.5 mM ionic strength. In each experiment, three identical columns with the same initial 260 min input pulse of bacteria were stopped at different times and the retained bacteria were extracted (bottom). The solid line depicts the predictions of the model that was fit to the longest duration column experiment. Error bars represent the upper and lower 95% confidence interval.

3.3. Extended Duration Experiments With Repacked Drill Cuttings

[36] The drill cuttings used in the extended duration experiments DCE-1 and DCE-2 were taken from depths of 15.2–18.3 m and 7.6–10.6 m, respectively, and both have uniformity coefficients below 3 (Table 1). DCE-1 cuttings had a grain size of 0.183 mm, while the DCE-2 cuttings had a smaller average grain size of 0.118 mm. Each test series consisted of three individual packed columns run simultaneously but stopped at different times.

[37] Experiments DCE-3.5-1 a to c (Figure 4a) had the highest normalized breakthrough concentrations of any unwashed drill cuttings tested, rising from approximately 0.3 to 0.4 over the course of the contamination phase. The column experiments in this series were terminated after 610, 2035, and 4122 min, respectively. Normalized effluent concentrations in these experiments exceeded 0.03 for over 500 min after the switch back to clean AGW and did not fall below the detection limit for the duration of the experiment. In each of these experiments the two-population model was preferred, based on the reduction in the AIC (Table 3). The fitted reversible attachment and detachment rates were zero for the column that was stopped immediately after switching to clean solution (DCE-3.5-1a). As in other experiments that were fit with the two-population model, the DCE-3.5-1 series had a second population with a very small irreversible attachment rate, as compared to the primary population.

[38] Experiments DCE-3.5-2 a to c had a lower normalized breakthrough concentration compared to the DCE-3.5-1 series, rising from 0.1 to 0.2, with significant detachment also occurring after the switch back to clean solution. These columns were stopped after 505, 1280, and 3360 min, respectively. The retained particle profiles of experiments DCE-3.5-2 a and b were more difficult to fit (adjusted $R^2 = 0.75$ and 0.88) due to secondary peaks between dimensionless depths of 0.6 and 0.8. However, the longest experiment did not exhibit this phenomenon and was fit well by the single-population model (adjusted $R^2 = 0.98$). Only one experiment in the DCE-3.5-2 series required a second population to obtain reasonable agreement between the modeled and observed results (DCE-3.5-2b).

3.4. Decay Experiment

[39] Concentrations of *E. coli* in three controls containing liquid without sediment remained steady or increased slightly in concentration over the first 2 days of the experiment before beginning a slow decrease from an average of 6.7×10^4 at day 1 to 4.3×10^4 CFU/100 mL at day 7 (Figure 5a). The corresponding first-order decay rate for the liquid phase was 0.029 $\log_{10}$/day ($R^2 = 0.65$).

[40] In samples with sediment and water, the concentration of *E. coli* in the aqueous phase increased in concentration from day 0 to day 1 by an average of 48% (Figure 5b). This initial increase in concentration was not observed in the liquid-only controls and was attributed to the detachment of particles that were hydrodynamically retained following the 30 min agitation phase of the experiment. After the day 1 observations, the concentration of *E. coli* decreased in an approximately log-linear fashion consistent with first-order decay. The average correction made due to attachment of bacteria after the test began was between 2 and 12% of the overall solid-phase concentration, with the exception of tube 2C, which had a much lower number of extracted bacteria than any other tube and was determined

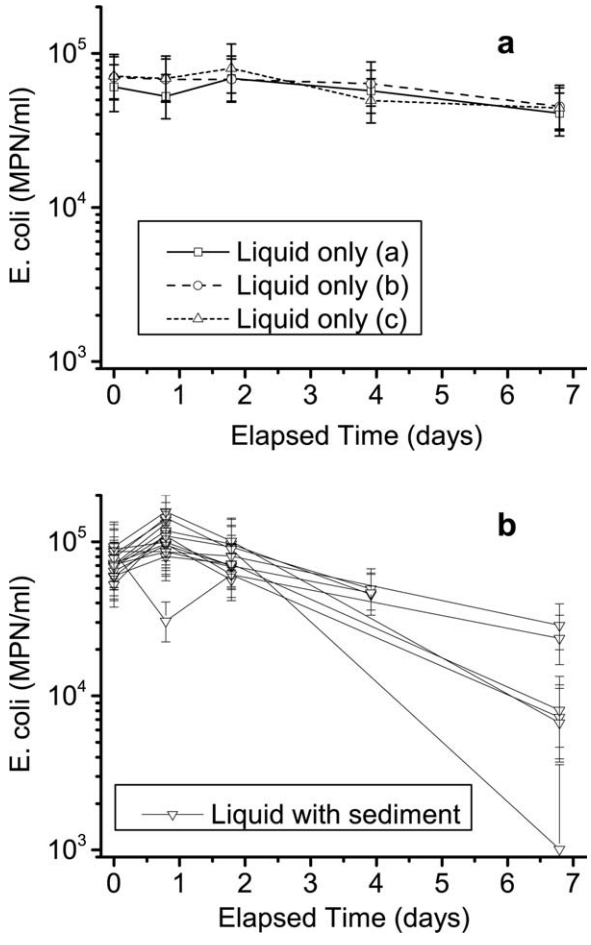

Figure 5. Liquid-phase *E. coli* concentrations during a 7 day incubation at room temperature (a) in tubes containing pure AGW and (b) in tubes with sediment added.

to be an outlier. Solid-phase concentrations of *E. coli* varied between 2.3 to 3.6 $\times$ 10^5 CFU/mL (Figure 6), with the exception of the outlier (tube 2C). A linear regression on the logarithm of the corrected solid-phase concentrations results in a solid-phase decay rate of 0.031 $\log_{10}$/day.

3.5. Trends in Fitted Parameters

[41] Trends in the fitted parameters using the single-population model for the low ionic strength experiments with unwashed sediments are shown in Figure 7 as a function of average grain diameter, D_{50}. The high ionic strength columns are excluded here because very little breakthrough was observed for most of these experiments, which means these conditions are unlikely to be important in understanding long-distance transport of bacteria in aquifers. The single irreversible rate model is equivalent to classical CFT and is a useful measure of the average breakthrough concentration for each experiment. The reversible and irreversible attachment rates decrease with increasing grain diameter for both repacked and sediment cores alike. In contrast, the detachment rate did not vary systematically with grain size or any other physical parameter of the sediment measured during this research work. All of the attachment rates (k_a, k_i, and k_{CFT}) increase with increasing percent fines. The trend is most apparent for k_{CFT} (Figure 7h), where a linear increase ($R^2 = 0.92$) is observed for all of the sediment types tested at low ionic strength.

[42] The relationship between the grain size distribution and the utility of employing a second population in modeling the experiment results is examined in Figure 8. An improvement in the goodness of fit statistic (adjusted R^2) after switching from a single-population to a two-population model is only observed above a grain size of approximately 0.175 mm. The percent fines show an inverse relationship, with increases in the adjusted R^2 appearing to increase dramatically below 2.5% fines (Figure 8a).

3.6. Transport Simulations

[43] In order to help understand the contribution of vertical transport to the high levels of bacterial contamination observed at the field site in Bangladesh where the sediments were extracted, several simulations were conducted using the same pore velocity and model parameters as the column experiments, but with the transport distance extended to 10 m to represent the typical distance from a fecal contamination source to a tubewell. The simulations assume a constant source, such as a contaminated pond or latrine. Very little transport occurs using the parameters obtained from column experiments that were fit to a single-population dual-deposition model (Figures 9a and 9b). Even at the lower range of attachment rates observed, after 30 days of simulated transport, the concentration is reduced by 4 orders of magnitude within the first meter of transport below the source. However, when a second population (making up 30% of the total) of low irreversibly attaching bacteria is added, concentrations can reach up

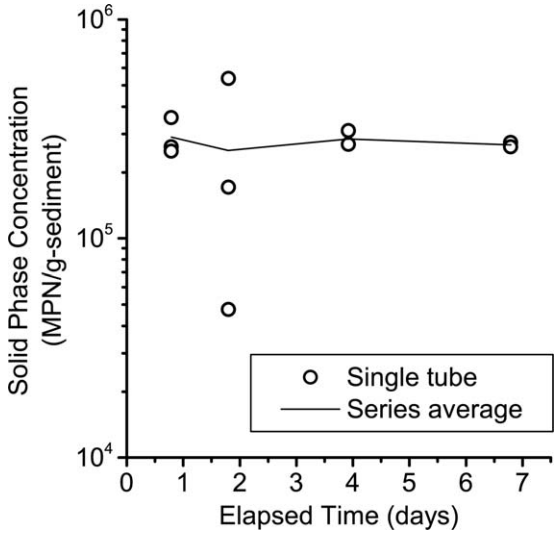

Figure 6. Solid-phase *E. coli* concentrations of individual sediment tubes versus time spent stored in the dark at room temperature in 3.5 mM simulated groundwater. Concentrations were corrected for subsequent reattachment (2–12% total correction). Circles represent individual data points (three per time interval, some points overlap), and the solid line is the average for each series.

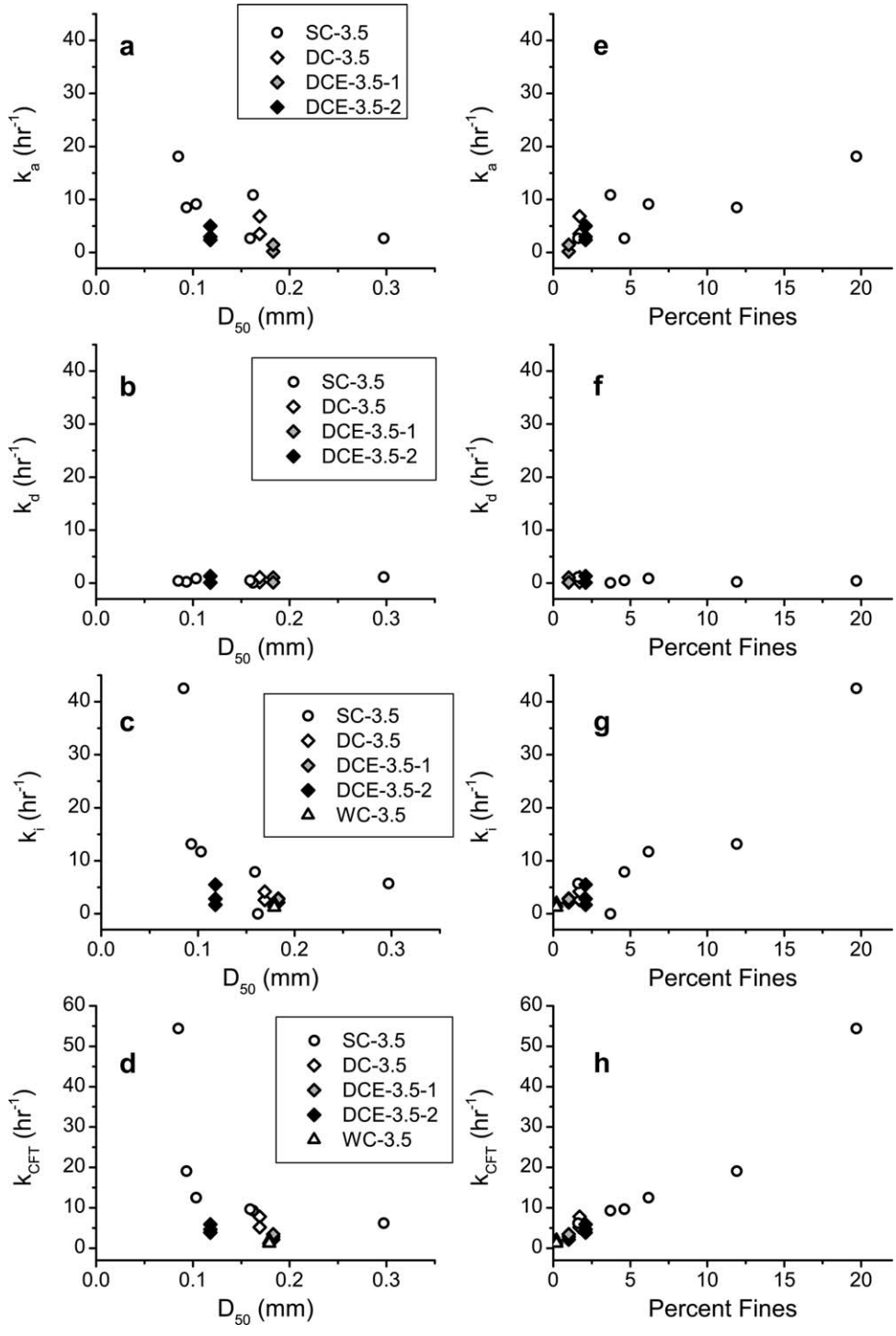

Figure 7. Trends in modeled parameters for column experiments conducted at 3.5 mM ionic strength fitted with a single population dual-deposition model (a–c and e–g) or a single irreversible attachment rate (CFT) model (d and h), as a function of average grain diameter (D_{50}) (left-hand side) or percent fine material (right-hand side). The parameters plotted are reversible attachment rate (k_a), detachment rate (k_d), irreversible attachment rate (k_i), and a single lumped irreversible attachment rate based on the assumptions of colloid filtration theory (k_{CFT}).

to 1% of the influent level at nearly 10 m (Figures 9c and 9d). As the length of the simulation increases, the liquid-phase concentration profile reaches an asymptote, whose slope is defined by the decay rate of the bacteria in the liquid phase and in the reversible solid-phase attachment sites.

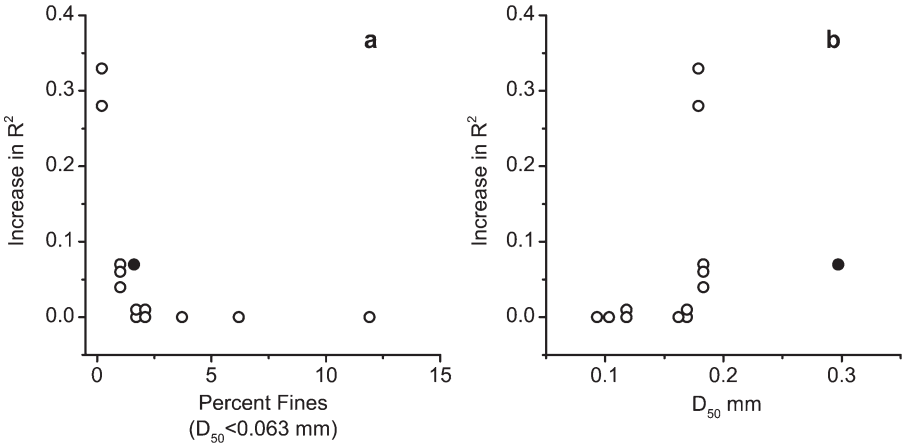

Figure 8. Difference in goodness of fit parameter (adjusted R^2) between two-population and one-population models fit to low ionic strength (3.5 m*M*) column experiments as a function of percent fine material ($D_{50} < 0.063$ mm) and average grain diameter, D_{50}. The filled-in circle (SC-3.5-4), while an outlier with respect to grain diameter, fits the overall trend with respect to percent fines.

4. Discussion

4.1. Effects of Grain Size and Sediment Layering

[44] There was significant variability in the grain sizes and percent fine material across all the sediment cores tested. Independent of grain size, the repacked cores (WC and DC) always had higher breakthrough concentrations and lower retained concentrations than the intact sediment cores (SC). For example, core SC-3.5-4 had the highest overall grain size found in any experiment but still had a normalized breakthrough concentration of only 5%. The fine layering in at least two of these intact cores (Figure 1) provides additional evidence that physical heterogeneity may be driving the lower overall breakthrough found in intact cores. In the column experiments, fluid flow was one dimensional and forced in a perpendicular direction to sediment layering; whereas in the field groundwater flow is also lateral and influenced by physical heterogeneity [*Dong et al*., 2002; *Mailloux et al*., 2003; *Bradford et al*., 2004; *Zheng et al*., 2011]. Therefore, predicting field transport using one-dimensional sediment columns may obscure the contribution of multiple attachment sites and multiple populations on aquifer-scale transport.

4.2. Occurrence of a Second Population of Low-Attaching Bacteria

[45] Multiple studies have found it necessary to include two bacterial populations in order to simultaneously fit both breakthrough and retained profiles [*Simoni et al*., 1998; *Yoon et al*., 2006; *Foppen et al*., 2007a], and the rates determined are generally in agreement with the current study when obtained under similar conditions. In experiments using glass beads with *E. coli*, breakthrough and retained profiles could be fit by two populations; the first population (making up between 50 and 70% of the total) had attachment rates between 102 and 227 h^{-1}, and the second, low-attaching population had much lower rates between 0.6 and 10 h^{-1} [*Foppen et al*., 2007a]. Similarly, the washed sediment experiments (WC) were best fit by a higher attaching population with rates between 24 and 33 h^{-1} and a second population (between 14 and 60% of the total) with low attachment rates between 0.3 and 0.48 h^{-1}. In a separate study, *Foppen et al*. [2007b] used a dual-deposition mode approach for *E. coli* attachment with deionized water in washed quartz sand to fit profiles for strained and adsorbed bacteria separately, finding a reversible attachment rate between 3 and 22 h^{-1} and an irreversible rate between 25 and 350 h^{-1}. Tong and coworkers applied a random-walk particle tracking model to transport of an adhesion-deficient bacterial strain in soda-lime glass beads, finding attachment rates between 0.2 and 1.6 h^{-1} and detachment rates between 0.05 and 0.25 h^{-1} [*Tong et al*., 2005]. These rates are comparable to all of the low ionic strength experiments in the current study, where the average detachment rate was 0.5 h^{-1}. Interestingly, *Tong et al*. [2005] also reported peaks in retained bacteria toward the middle or end of the column that could not be fit by their model, which is similar to the phenomenon observed in the DCE-2 extended duration experiments (Figure 4). By manipulating the parameters in the finite difference model used in the current study, it was possible to produce simulations in which a short-lived retained concentration peak moved from the inlet to the outlet of a column but the parameter estimation routines could not fit such peaks in the experimental data.

[46] Some important simplifying assumptions about rate parameters and population distribution were made in order to fit the experimental results of the current study. The decision to fit a second population with reversible attachment and detachment rates that are fixed to the first population rates allowed the elimination of two fitting parameters. This approach was motivated by the need to fit the hyperexponential retained bacteria profiles (Figures 2–4), which could be reproduced by varying the irreversible attachment rates since most of the retained bacteria in the column at the end of the experiment are irreversibly attached. While other studies have employed dual-deposition kinetic attachment rates, one of which is often attributed to straining [*Foppen et al*., 2007b; *Bradford et al*., 2005], these have been conducted in very clean sand with negligible detachment rates. The unwashed sediments of the present study, most notably the intact cores, all exhibited some degree of

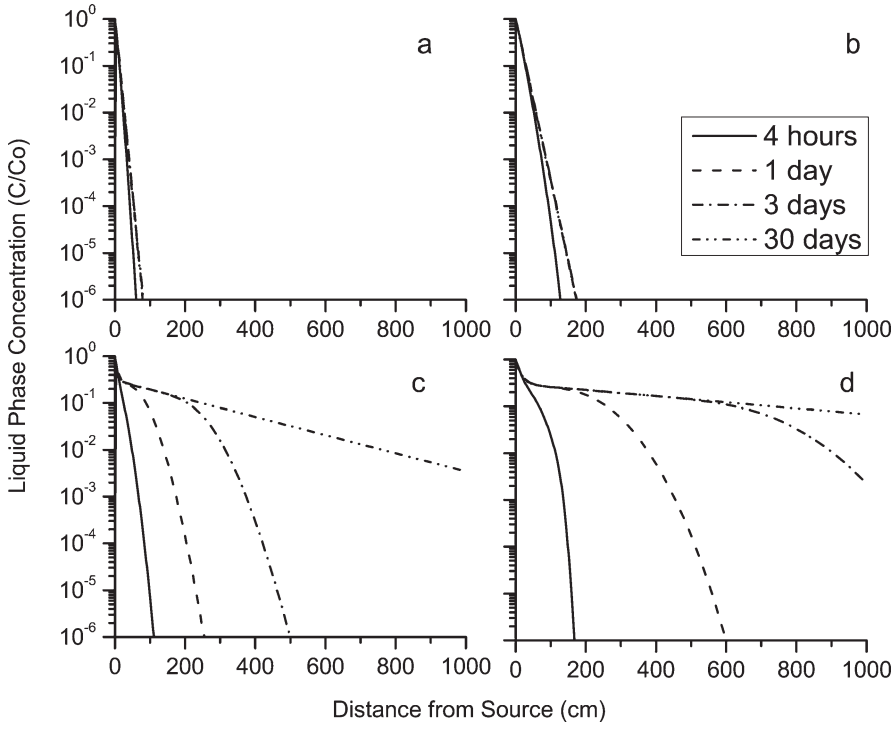

Figure 9. Simulations of liquid-phase bacteria concentrations over a distance of 10 m and pore water velocity of 0.5 cm/min. (a and b) Transport assuming a single-population dual-deposition model with typical parameter values (Figure 8a: $k_a = 4.8$, $k_d = 0.6$, $k_i = 5.4\ h^{-1}$) and low values (Figure 8b: $k_a = 1.2$, $k_d = 0.6$, $k_i = 2.4\ h^{-1}$). (c and d) Transport assuming a two-population model with typical values (Figure 8c: $k_a = 4.8$, $k_d = 0.6\ h^{-1}$, 70% of population with $k_i = 5.4\ h^{-1}$ and 30% of population with $k_i = 0$) and low values (Figure 8d: $k_a = 1.2$, $k_d = 0.6\ h^{-1}$, 70% of population with $k_i = 2.4\ h^{-1}$ and 30% of population with $k_i = 0$).

detachment behavior as evidenced by the rising plateaus in the loading phase (Figures 2 and 3) and the long tails in the deloading phase (Figure 4). The extended tails in log-transformed virus breakthrough curves have been used to extract two separate detachment rates [*Schijven et al*., 2002], but this was not attempted in the present study because relatively few experiments of sufficient duration were carried out.

[47] Finally, it should be noted that others have successfully applied continuous distributions to account for variations in irreversible attachment rates using the CFT model, to include an α distribution [*Abramson and Brown*, 2007], lognormal distribution [*Tong and Johnson*, 2007], and a power-law relationship [*Lutterodt et al*., 2011]. While these approaches may more closely represent the natural variability in bacteria properties [*Bolster et al*., 2000], it would not be feasible to fit distribution means and shape parameters for each of the three rates needed to fit the experimental results in this study so this was not attempted.

4.3. Conditions Conducive to Observing Population Heterogeneity

[48] The lack of any reversible attachment occurring in the washed sediment indicates that the reversible attachment observed in these experiments is related to geochemical heterogeneity. To confirm the difference in geochemical makeup of the drill cuttings, the iron content was measured by hot extraction with 1.2 *M* HCl at 80°C. The unwashed drill cuttings had 8700 ppm (mass iron/mass sediment) extractable iron, whereas the washed cuttings only had 800 ppm. The washed cuttings and some repacked and intact cores required the model with two populations due to their hyperexponential retained particle profiles, providing some evidence that the two-population phenomenon is not due to geochemical heterogeneity of attachment sites.

[49] While the diversity of sediments used in this study was small and inherently limited by the diversity present in the drilled samples collected from the aquifer, it is possible with the experimental results presented in this paper to begin to constrain the sediment types where the two-population behavior is likely to be observed at the scale of these experiments (12 cm). The inflection points at which the two-population model is favored were at average grain sizes above 0.175 mm and at percent fines below 2.5% (Figure 8). Taken together, these two findings point toward sediments with relatively large grain diameter and very little fine material as providing conditions most conducive to the observation of two populations, one of which has a reduced attachment rate that is more favorable to long-distance transport.

4.4. Implications of the Two-Population Model

[50] The two-population model and the parameters determined in this study have important practical implications for the safety of untreated groundwater from shallow

aquifers. First, sediments whose fraction of fine material was lower than 2.5% were most likely to require the two-population approach to fit the data. Percent fines is simple to measure in the field using a single sieve and could therefore be useful to local drillers and septic installers in assessing the relative risk of different sediment types. Likewise, the electrical conductivity can easily be measured relatively inexpensively. The upper dissolved ion concentration tested in this study of 20 mM KCl produced irreversible attachment rates that were four to five times higher than comparable experiments conducted at 3.5 mM. As a result, decreases in ionic strength caused by seasonal changes in surface water flux would be expected to result in the release of attached bacteria.

[51] The simulations (Figure 9) show that the two-population model has very different implications for long distance transport, yet the liquid-phase concentrations remain very similar over the first meter of transport away from the source. These results underscore the importance of measuring the solid-phase concentration profile of attached bacteria in order to constrain the type of model to be applied. In sediment types where two-population behavior occurs, the solid- and liquid-phase decay rates may be the key parameters in determining the safety of drinking water from shallow tube wells.

5. Conclusions

[52] In this study, the transport of *E. coli* at concentrations of approximately 10^6 CFU/mL in electrolyte solutions at two ionic strengths, 3.5 and 20 mM, was compared in columns of repacked, dried drill cuttings; repacked, acid-washed drill cuttings, and intact sediment cores that were obtained from a shallow aquifer in Bangladesh. When the rates obtained from all low ionic strength experiments (the most relevant conditions for long-distance transport) were compared as a function of both average grain size and percent fines, it was observed that all attachment rates (reversible and irreversible) increase linearly with percent fines. A two-population dual-deposition mode model was required to fit one third of the experiments, which tended to have a larger average particle diameter and low percentage of fine material. Simulations using a two-population model with parameters found in these experiments show that bacterial concentrations would rapidly decrease within the first meter of transport but would decrease at a much slower rate over distances up to 10 m because of the low irreversible attachment rate of the second population. In these situations, long-distance transport of *E. coli* is determined mainly by decay rates.

[53] **Acknowledgments.** This study was supported by NIH/Forgarty International Center grant 5R01TW8066-2. We are grateful to Dhaka University students Mohammad Rezaul Huq and Mohammad Jahangir Alam for their expertise and support in the field.

References

Abramson, A., and D. G. Brown (2007), Influence of solution ionic strength on the collision efficiency distribution and predicted transport distance of a Sphingomonas sp. flowing through porous media, *Water Res.*, *41*(19), 4435–4445, doi:10.1016/j.watres.2007.06.005.

Akaike, H. (1974), A new look at the statistical model identification, *IEEE Trans. Autom. Control*, *19*(6), 716–723, doi:10.1109/TAC.1974.1100705.

Bales, R. C., S. Li, T. J. Yeh, M. E. Lenczewski, and C. P. Gerba (1997), Bacteriophage and microsphere transport in saturated porous media: Forced-gradient experiment at Borden, Ontario, *Water Resour. Res.*, *33*, 639–648.

Basha, H. A., and P. J. Culligan (2010), Modeling particle transport in downward and upward flows, *Water Resour. Res.*, *46*, W07518, doi:10.1029/2009WR008133.

Bolster, C. H., A. L. Mills, G. Hornberger, and J. Herman (2000), Effect of intra-population variability on the long-distance transport of bacteria, *Ground Water*, *38*(3), 370–375.

Bopp, D. J., B. D. Sauders, A. L. Waring, J. Ackelsberg, N. Dumas, E. Braun-Howland, D. Dziewulski, B. J. Wallace, M. Kelly, and T. Halse (2003), Detection, isolation, and molecular subtyping of *Escherichia coli* O157: H7 and *Campylobacter jejuni* associated with a large waterborne outbreak, *J. Clin. Microbiol.*,*41* (1), 174–180.

Bradford, S. A., M. Bettahar, J. Simunek, and M. T. van Genuchten (2004), Straining and attachment of colloids in physically heterogeneous porous media, *Vadose Zone J.*, *3*(2), 384–394.

Bradford, S. A., J. Simunek, M. Bettahar, Y. F. Tadassa, M. T. van Genuchten, and S. R. Yates (2005), Straining of colloids at textural interfaces, *Water Resour. Res.*, *41*, W10404, doi:10.1029/2004WR003675.

Brown, D. G., and A. Abramson (2006), Collision efficiency distribution of a bacterial suspension flowing through porous media and implications for field-scale transport, *Water Res.*, *40*(8), 1591–1598, doi:10.1016/j.watres.2006.02.016.

Dong, H., T. C. Onstott, M. F. DeFlaun, M. E. Fuller, T. D. Scheibe, S. H. Streger, R. K. Rothmel, and B. J. Mailloux (2002), Relative dominance of physical versus chemical effects on the transport of adhesion-deficient bacteria in intact cores from South Oyster, Virginia, *Environ. Sci. Technol.*, *36*(5), 891–900.

Dong, H., T. D. Scheibe, W. P. Johnson, C. M. Monkman, and M. E. Fuller (2006), Change of collision efficiency with distance in bacterial transport experiments, *Ground Water*, *44*(3), 415–429, doi:10.1111/j.1745–6584.2005.00133.

Ferguson, A. S., et al. (2012), Comparison of fecal indicators with pathogenic bacteria and rotavirus in groundwater, *Sci. Total Environ. C*, *431*, 314–322, doi:10.1016/j.scitotenv.2012.05.060.

Fitzpatrick, J. A., and L. A. Spielman (1973), Filtration of aqueous latex suspensions through beds of glass spheres, *J. Colloid Interface Sci.*, *43*(2), 350–369.

Foppen, J. W. A., and J. F. Schijven (2006), Evaluation of data from the literature on the transport and survival of *Escherichia coli* and thermotolerant coliforms in aquifers under saturated conditions, *Water Res.*, *40*(3), 401–426, doi:10.1016/j.watres.2005.11.018.

Foppen, J. W., M. van Herwerden, and J. Schijven (2007a), Transport of *Escherichia coli* in saturated porous media: Dual mode deposition and intra-population heterogeneity, *Water Res.*, *41*(8), 1743–1753.

Foppen, J. W., M. V. Herwerden, and J. Schijven (2007b), Measuring and modelling straining of *Escherichia coli* in saturated porous media, *J. Contam. Hydrol.*, *93*(1–4), 236–254, doi:10.1016/j.jconhyd.2007.03.001.

Happel, J. (1958), Viscous flow in multiparticle systems: Slow motion of fluids relative to beds of spherical particles, *AIChE J.*, *4*(2), 197–201.

Harvey, R. W., L. H. George, R. L. Smith, and D. R. LeBlanc (1989), Transport of microspheres and indigenous bacteria through a sandy aquifer: Results of natural- and forced-gradient tracer experiments, *Environ. Sci. Technol.*, *23*(1), 51–56.

Harvey, R. W., N. E. Kinner, D. MacDonald, D. W. Metge, and A. Bunn (1993), Role of physical heterogeneity in the interpretation of small-scale laboratory and field observations of bacteria, microbial-sized microsphere, and bromide transport through aquifer sediments, *Water Resour. Res.*, *29*(8), 2713–2722.

Johnson, W. P., X. Li, and S. Assemi (2007a), Deposition and re-entrainment dynamics of microbes and non-biological colloids during non-perturbed transport in porous media in the presence of an energy barrier to deposition, *Adv. Water Resour.*, *30*(6–7), 1432–1454.

Johnson, W. P., X. Li, and G. Yal (2007b), Colloid retention in porous media: Mechanistic confirmation of wedging and retention in zones of flow stagnation, *Environ. Sci. Technol.*, *41*(4), 1279–1287.

Katayama, H. (2008), Detection of microbial contamination in groundwater, in *cSUR-UT Series: Library for Sustainable Urban Regeneration*, vol. *2*, edited by Satoshi Takizawa, pp. 151–169, Springer, Japan.

Khan, S. R., and B. Islam (2008), Holocene stratigraphy of the lower Ganges-Brahmaputra river delta in Bangladesh, *Frontiers Earth Sci. China*, *2*(4), 393–399, doi:10.1007/s11707-008-0051-8.

Knappett, P. S., et al. (2012), Implications of fecal bacteria input from latrine-polluted ponds for wells in sandy aquifers, *Environ. Sci. Technol.*, *46*(3), 1361–1370, doi:10.1021/es202773w.

Li, X., C. L. Lin, J. D. Miller, and W. P. Johnson (2006), Role of grain-to-grain contacts on profiles of retained colloids in porous media in the presence of an energy barrier to deposition, *Environ. Sci. Technol.*, *40*(12), 3769–3774.

Li, X. Q., Z. L. Li, and D. X. Zhang (2010), Role of low flow and backward flow zones on colloid transport in pore structures derived from real porous media, *Environ. Sci. Technol.*, *44*(13), 4936–4942, doi:10.1021/es903647g.

Litton, G. M., and T. M. Olson (1993), Colloid deposition rates on silica bed media and artifacts related to collector surface preparation methods, *Environ. Sci. Technol.*, *27*(1), 185–193.

Liu, C., and J. B. Evett (2003), *Soil Properties: Testing, Measurements, and Evaluation*, 5th ed., Prentice Hall, Upper Saddle River, NJ.

Logan, B. E., D. G. Jewett, R. G. Arnold, E. J. Bouwer, and C. R. O'Melia (1995), Clarification of clean-bed filtration models, *J. Environ. Eng.*, *121*(12), 869–873.

Lutterodt, G., J. W. A. Foppen, A. Maksoud, and S. Uhlenbrook (2011), Transport of *Escherichia coli* in 25 m quartz sand columns, *J. Contam. Hydrol.*, *119*, 80–88, doi:10.1016/j.jconhyd.2010.09.010.

Mailloux, B. J., et al. (2003), The role of physical, chemical, and microbial heterogeneity on the field-scale transport and attachment of bacteria, *Water Resour. Res.*, *39*(6), 1142, doi:10.1029/2002WR001591.

Olsen, S. J., G. Miller, T. Breuer, M. Kennedy, C. Higgins, J. Walford, G. McKee, K. Fox, W. Bibb, and P. Mead (2002), A waterborne outbreak of *Escherichia coli* O157:H7 infections and hemolytic uremic syndrome: Implications for rural water systems, *Emerg. Infect. Dis.*, *8*(4), 370–375.

Pang, L., M. McLeod, J. Aislabie, J. Simunek, M. Close, and R. Hector (2008), Modeling transport of microbes in ten undisturbed soils under effluent irrigation, *Vadose Zone J.*, *7*(1), 97–111, doi:10.2136/vzj2007.0108.

Rajagopalan, R., and C. Tien (1976), Trajectory analysis of deep-bed filtration with the sphere-in-cell porous media model, *AIChE J.*, *22*(3), 523–533.

Redman, J. A., S. L. Walker, and M. Elimelech (2004), Bacterial adhesion and transport in porous media: Role of the secondary energy minimum, *Environ. Sci. Technol.*, *38*(6), 1777–1785.

Richardson, H. Y., G. N. Nichols, C. L. Lane, I. R. L. Lake, and P. R. H. Hunter (2009), Microbiological surveillance of private water supplies in England—The impact of environmental and climate factors on water quality, *Water Res.*, *43*(8), 2159–2168, doi:10.1016/j.watres.2009.02.035.

Scheibe, T. D., S. S. Hubbard, T. C. Onstott, and M. F. Deflaun (2011), Lessons learned from bacterial transport research at the South Oyster Site, *Ground Water*, *49*(5), 1–19, doi:10.1111/j.1745–6584.2011.00831.x.

Schets, F. M., M. During, R. Italiaander, L. Heijnen, S. A. Rutjes, W. K. van der Zwaluw, and A. M. de Roda Husman (2005), *Escherichia coli* O157:H7 in drinking water from private water supplies in the Netherlands, *Water Res.*, *39*(18), 4485–4493, doi:10.1016/j.watres.2005.08.025.

Schijven, J. F., S. M. Hassanizadeh, and R. H. de Bruin (2002), Two-site kinetic modeling of bacteriophages transport through columns of saturated dune sand, *J. Contam. Hydrol.*, *57*(3–4), 259–279.

Simoni, S. F., H. Harms, T. N. P. Bosma, and A. J. B. Zehnder (1998), Population heterogeneity affects transport of bacteria through sand columns at low flow rates, *Environ. Sci. Technol.*, *32*(14), 2100–2105.

Simunek, J., and J. W. Hopmans (2002), Parameter optimization and nonlinear fitting, in *Methods of Soil Analysis. Part 1, Physical Methods, SSSA*, Madison, WI, vol. *4*, pp. 139–157.

Slutsker, L., A. A. Ries, K. Maloney, J. G. Wells, K. D. Greene, and P. M. Griffin (1998), A nationwide case-control study of *Escherichia coli* O157:H7 infection in the United States, *J. Infect. Dis.*, *177*(4), 962–966.

Tong, M., and W. P. Johnson (2007), Colloid population heterogeneity drives hyperexponential deviation from classic filtration theory, *Environ. Sci. Technol.*, *41*(2), 493–499.

Tong, M., X. Li, C. N. Brow, and W. P. Johnson (2005), Detachment-influenced transport of an adhesion-deficient bacterial strain within water-reactive porous media, *Environ. Sci. Technol.*, *39*(8), 2500–2508.

Toride, N., F. J. Leij, and M. Van Genuchten (1995), The CXTFIT code for estimating transport parameters from laboratory or field tracer experiments, Ver. 2.0, US Salinity Laboratory, USDA, Riverside, CA, *Res. Rep. 137*.

Tufenkji, N. (2007), Modeling microbial transport in porous media: Traditional approaches and recent developments, *Adv. Water Resour.*, *30*(6–7), 1455–1469.

Tufenkji, N., and M. Elimelech (2004), Deviation from the classical colloid filtration theory in the presence of repulsive DLVO interactions, *Langmuir*, *20*(25), 10,818–10,828.

Tufenkji, N., and M. Elimelech (2005), Breakdown of colloid filtration theory: Role of the secondary energy minimum and surface charge heterogeneities, *Langmuir*, *21*(3), 841–852.

van Geen, A., et al. (2011), Fecal contamination of shallow tubewells in Bangladesh inversely related to arsenic, *Environ. Sci. Technol.*, *45*(4), 1199–1205, doi:10.1021/es103192b.

Yao, K. M., M. T. Habibian, and C. R. O'Melia (1971), Water and waste water filtration. Concepts and applications, *Environ. Sci. Technol.*, *5*(11), 1105–1112, doi:10.1021/es60058a005.

Yoon, J. S., J. T. Germaine, and P. J. Culligan (2006), Visualization of particle behavior within a porous medium: Mechanisms for particle filtration and retardation during downward transport, *Water Resour. Res.*, *42*, W06417, doi:10.1029/2004WR003660.

Zheng, C., M. Bianchi, and S. M. Gorelick (2011), Lessons learned from 25 years of research at the MADE site, *Ground Water*, *49*(5), 649–62, doi:10.1111/j.1745–6584.2010.00753.x.